Formation of Ultrarelativistic Electron Rings from a Laser-Wakefield Accelerator

B. B. Pollock, F. S. Tsung, F. Albert, J. L. Shaw, C. E. Clayton, A. Davidson, N. Lemos, K. A. Marsh, A. Pak, J. E. Ralph, W. B. Mori, and C. Joshi

Phys. Rev. Lett. **115**, 055004 — Published 31 July 2015

DOI: 10.1103/PhysRevLett.115.055004

Formation of ultra-relativistic electron rings from a laser wakefield accelerator

B. B. Pollock,[1,*] F. S. Tsung,[2] F. Albert,[1] J. L. Shaw,[2] C. E. Clayton,[2] A. Davidson,[2]
N. Lemos,[2] K. A. Marsh,[2] A. Pak,[1] J. E. Ralph,[1] W. B. Mori,[2] and C. Joshi[2]

[1] *Lawrence Livermore National Laboratory, 7000 East Ave., Livermore, CA 94550*
[2] *University of California, Los Angeles, 405 Hilgard Ave., Los Angeles, CA 90095*

Ultra-relativistic-energy electron ring structures have been observed from laser wakefield acceleration experiments in the blowout regime. These electron rings had 170-280 MeV energies with 5-25% energy spread and ∼10 pC of charge and were observed over a range of plasma densities and compositions. 3-D PIC simulations show that laser intensity enhancement in the wake leads to sheath splitting and the formation of a hollow toroidal pocket in the electron density around the wake behind the first wake period. If the laser propagates over a distance greater than the ideal dephasing length, some of the dephasing electrons in the second period can become trapped within the pocket and form an ultra-relativistic electron ring that propagates in free space over a meter-scale distance upon exiting the plasma. Such a structure acts as a relativistic potential well, which has applications for accelerating positively-charged particles such as positrons.

PACS numbers: 52.38.Kd, 41.75.Jv, 52.35.Mw

Relativistic electron rings were originally proposed [1] for collective acceleration of ions in conventional radiofrequency (RF) accelerators [2], then as improved drivers [3] for plasma-based wakefield acceleration of positrons [4], and later as drivers for a two-beam accelerator [5]. More recently, lower-energy electron rings have been used in RF accelerators as compact collimators for proton bunches [6]. Recent simulations have shown that such high-energy electron rings can be produced and accelerated by donut-shaped wakefields driven by Laguerre-Gaussian laser pulses [7]. In this Letter, we demonstrate that laser wakefield accelerators (LWFAs) [8] driven by Gaussian-like laser pulses can also produce highly-relativistic spatial rings of electrons in addition to their characteristic, on-axis electron beams [9–12]. The generation of such electron rings in this experiment is explained using three-dimensional (3-D) particle-in-cell (PIC) simulations, where the ring formation depends on the dynamic evolution of the laser pulse and the plasma wave. Direct measurements of the processes involved are not currently possible; however, understanding the origin of structures such as the electron rings described herein provides potential diagnostic applications for these features.

LWFA occurs when a short, relativistically-intense laser pulse is focused into a low-density gas or preformed underdense plasma. To access the blowout regime [13] of LWFA, the pulse duration $c\tau$ should be equal to the blowout radius, which is $\geq \lambda_p = 2\pi c/\omega_p$, and the laser's normalized vector potential $a_0 = eA/mc$ must satisfy $2 < a_0 < 2\omega_0/\omega_p$. Here, A is the laser vector potential, ω_0 is the laser angular frequency, and $\omega_p = \sqrt{n_e e^2/\epsilon_0 m_e}$ is the electron plasma frequency with n_e the electron density. Consequently, gas is readily ionized via tunnel ionization and plasma electrons at the front of the laser pulse are expelled from the laser axis by its transverse ponderomotive force. As a result of this near-complete electron expulsion, a region containing only the more massive ions (immobile on such short timescales τ <100 fs) is formed near the axis. The laser continues propagating through the plasma, and electrons behind the pulse are drawn back toward the axis by the space charge of the ions; these electrons overshoot, setting up the plasma wake. For laser power $P > P_c = (n_c/n_e)17GW$ and a matched laser spot size $w_0 = R_B = \sqrt{a_0}\lambda_p/\pi$ [13], the laser pulse can be self-guided to drive the plasma wake for 10's of Rayleigh lengths [14]. Here P_c is the critical power for relativistic self-focusing [15], n_c is the critical density for the laser wavelength, and R_B is the maximum radius of the blown-out region ("bucket").

In the blowout regime, simulations indicate that the electron plasma wave induced by the laser pulse persists for 5-10 periods before phase mixing of the returning electrons causes a loss of coherence in the wake structure. Electrons can become trapped in the first and subsequent buckets and undergo acceleration. Simulations shown in this Letter reveal that electrons trapped in the second bucket can eventually form a spatial ring structure as they interact with the dynamically-evolving first two buckets, where the evolution is due to laser self-focusing and electron dephasing. Here, we experimentally show the formation of ultra-relativistic electron rings with ΔE/E of 5-25%, expansion angles of ∼50-80 mrad, and ∼10 pC of charge as seen in the table of Fig. 1. In both the self- [16] and ionization-injection [17, 18] regimes of electron trapping, rings are observed when the plasma length exceeds the ideal dephasing length [13] so that the laser and wake have each undergone significant transverse and longitudinal evolution.

The experiments are conducted using the Ti:Sapphire Callisto laser system at the Lawrence Livermore National Laboratory, delivering up to 200 TW in a 60 fs pulse. The 800 nm laser beam is focused with an f/8, off-axis parabolic mirror to a 12 μm full-width at half-maximum

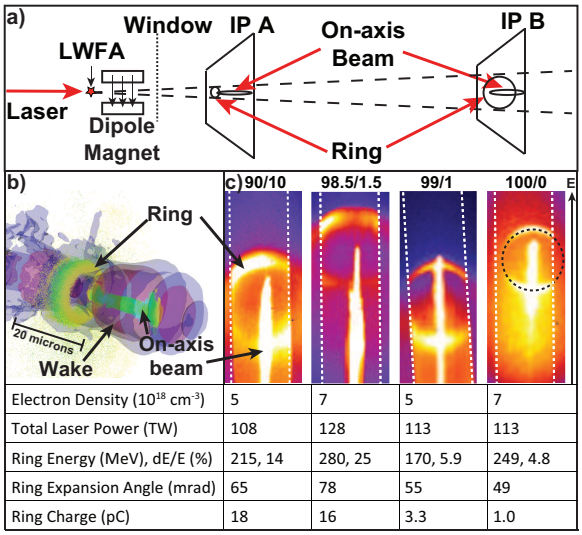

Electron Density (10^{18} cm^{-3})	5	7	5	7
Total Laser Power (TW)	108	128	113	113
Ring Energy (MeV), dE/E (%)	215, 14	280, 25	170, 5.9	249, 4.8
Ring Expansion Angle (mrad)	65	78	55	49
Ring Charge (pC)	18	16	3.3	1.0

FIG. 1. a) Top-view schematic of the electron spectrometer. The magnetic field is in the direction of the black arrows, causing electron dispersion out of the page. Two image plates (IP) record the electron flux exiting a vertically-slotted vacuum window, which is 2.5 cm (45 mrad) wide and consists of 50 μm-thick Al and 65 μm-thick mylar foils. This window partially blocks the full transverse width of the ring in the spectral images (dotted white lines). The magnet entrance is 3 cm from the plasma exit, and IP A (B) resides 62.2 (136.1) cm from the plasma exit. b) 3-D rendering from the OSIRIS simulation (see text) of the wake after 1 cm of plasma. The laser has been omitted for clarity. The solid blue-purple contours indicate the charge density of the wake structure, and the yellow-green dots represent the on-axis and the ring electrons accelerated in the wake. c) False-color raw (dispersion not linearized) images of IP A electron data sorted by the gas composition (%He/%N_2 by partial pressure, given above each image) from all of the cases where rings were produced in a 1 cm gas cell. The dotted black circle in the pure He case overlaps the ring. Table) Laser, target, and electron beam parameters for each image in (c). The charge quoted is that in the visible portion of the image that passes through the vacuum window.

(FWHM) spot (containing 50% of the power) at a position 500-750 μm inside a 10 mm-long gas cell target (~3 times the ideal dephasing length for the electron densities reported). The gas composition varied from pure He to He/N_2 mixtures containing up to 10% N_2 by partial pressure. The gas cell entrance (exit) aperture diameter is 500 μm (1 mm). For coupled powers of 30-60 TW (a_0=2-2.8), the LWFA process evolves from the forced wakefield [19] into the blowout regime. We have previously shown measurements of electron density and of self-guiding and spectral shifting of the laser pulse under similar conditions [20] indicating that the pulse propagates over an extended distance while forming a wake. After exiting the gas cell, electrons are dispersed by a 20 cm-long, 0.42 T dipole magnet, exit the vacuum chamber, and are recorded on two Fuji BAS-MS image plates (IP A and B) as shown in Fig. 1a.

The electron signal can consist of both an on-axis beam with a broad energy spectrum and narrow transverse width, and an electron ring. Figure 1b shows the 3-D structure of both of these electron features as obtained from the PIC simulation. The annular electron ring forms after 7 mm of laser propagation and resides at the back of the first wake bucket (discussed later). The experimentally-measured energy spectra of the on-axis and ring electrons on IP A are presented in Fig. 1c. Since features of each electron signal are present on both image plates, the energy and plasma exit angle of each feature are independently and uniquely determined following the procedure described in [21, 22]. This two-screen analysis yields a single exit angle from the vacuum laser axis for electrons in the broadband feature, where a typical spectrum is given in Fig. 2a. The continuous spectrum is consistent with previous observations utilizing ionization-injection because charge is continuously injected into the wake [9, 17, 20, 23]. Depending on the plasma composition, this broad feature can vary in its spectral peaks and maximum energy.

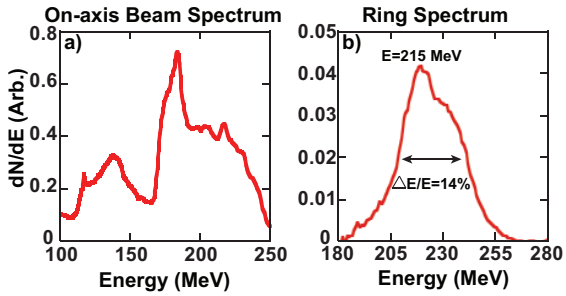

FIG. 2. Spectra for the a) broad energy on-axis beam with 41 mrad plasma exit angle and b) the "high-energy" side of the ring electron beam from the 90/10 gas composition data shown in Fig. 1c.

Applying the two-screen analysis to various positions around each ring gives the ring expansion angle (tabulated in Fig. 1) and the peak electron energy, which is azimuthally uniform within 5%. The spectrum in Fig. 2b corresponds to the bright, "high-energy" portion of the ring of Fig. 1c. Electrons with equal energies will all experience the same angular deflection when passing through the dipole magnet, preserving their initial spatial distribution. The data in Fig. 1c exhibit round rings after dispersion in the magnet, which together with the energy measurement implies that a round ring of electrons with a narrow energy spread compared with the peak energy entered the magnet. Although the peak energy is uniform, the energy spread can vary azimuthally, leading to some smearing of portions of the ring. Calculating the ring divergence angle directly from the separation of the image plates shows that the rings originate at the

plasma (as shown schematically in Fig. 1a); this divergence angle is consistent with the expansion angle from the energy analysis. The charge contained in the ring seems to generally increase with the N_2 percentage but the peak energy of the ring did not show any such correlation either to the nitrogen content or the peak energy of the on-axis electrons.

To understand the ring formation physics, 3-D OSIRIS [24] PIC simulations were performed for an a_0=2.8, 65 fs, 800 nm, 15 μm spot size laser pulse propagating through 1 cm of plasma with an electron density of 3×10^{18} cm^{-3}. This simulation utilizes a moving window [25] and includes ADK [26] tunnel-ionization of an initially-neutral mixture of 98%/2% He/N_2 gas. The simulation parameters are: box size = 800x1350x1350 c/ω_0 = 101.86x171.89x171.89 μm; grid = 4000x300x300; transverse resolution $k_p d_{x\perp}$=0.15; longitudinal resolution $k_0 d_{x\parallel}$=0.2; and 2 particles per cell per species.

Simulations show that ring formation occurs because electrons trapped in the second bucket interact with the dynamically-evolving wake structure. The wake needs to evolve into the nonlinear blowout regime [13, 16], where the ponderomotive force of the laser (or space charge force of an intense particle beam) nearly expels all of the plasma electrons. These electrons form a narrow sheath; for laser drivers, this sheath is not as well defined and it splits. Although not shown here, electron trajectories starting close to the axis cross those starting farther away from it. This splitting leads to the formation of toroidal pockets within the wake where relativistic electrons can be accelerated and guided off-axis. This process is shown in 2-dimensional slices of the 3-D electron density and laser pulse (Figs. 3a, 3c, and 3e) and the corresponding contour maps of the wake focusing/defocusing force, $\mathbf{F}_\perp$=-e$(\mathbf{E}+\mathbf{v_z}\times\mathbf{B})_\perp$ (3b, 3d, and 3f) from the simulation at 5, 7.5, and 10 mm of laser propagation. As seen in Fig. 3a (5 mm) ionization of the inner-shell N electrons has produced ionization-trapped charge inside the fully-formed wake, which is made up of He and outer-shell N electrons. The trapping condition for electrons born inside a non-evolving wake is [17] $\Delta\psi = -1+\sqrt{1+(p_{\perp f}/(m_e c))^2}/\gamma_\phi$, where $\psi \equiv \frac{e(\phi - v_\phi A_z)}{mc^2}$ is the normalized wake potential, $p_{\perp f}$ is the transverse momentum at the time of trapping, and γ_ϕ is the relativistic factor of the wake moving with phase velocity v_ϕ. Electrons with higher ionization potentials are born near the peak of the laser field (near the laser axis, e.g. from N_{6+}) and therefore have the largest initial ψ, allowing them to be more readily trapped in the first bucket. For these experimental parameters, γ_ϕ is sufficiently large initially that the trapping condition is essentially $\Delta\psi = -1$. Electrons born earlier in the laser pulse have a smaller initial ψ and, as they slip back to the edge of the first bucket, often do not satisfy the trapping condition. These electrons thus slip into the second bucket, where they have another chance to satisfy the trapping condition if the wake is evolving [27, 28]. The wake can evolve from a combination of beam loading of trapped electrons [29] and ponderomotive force enhancement from self-focusing and photon deceleration of the laser [30]. Both of these effects cause the radius of the first bucket to increase, moving the location of the wake potential minimum backward with respect to the laser pulse and reducing the effective wake phase velocity. This reduction is progressively greater in each successive bucket [31]. Therefore, electrons that could not satisfy the trapping condition in the first bucket can be trapped in later buckets as seen in Fig. 3a.

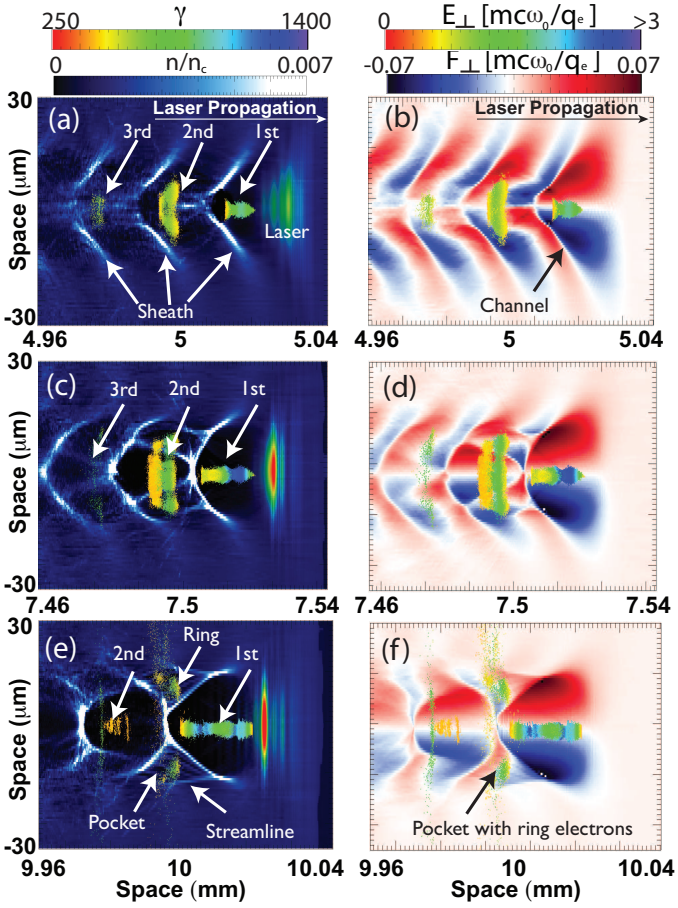

FIG. 3. a, c, e) Electron density maps from 3-D OSIRIS PIC simulations at 5, 7.5, and 10 mm of laser propagation, respectively. The $E_\perp$ color table corresponds to the envelope of the driving laser pulse at the right of the panels. b, d, f) Maps of the focusing force of the wake. White regions represent isocontours of zero focusing force. The key physical features are the electron sheath at the wake perimeter, the splitting of the sheath into outer and inner streamlines resulting in the formation of the toroidal pocket shown in (e), and the electrons trapped into each of the first two buckets close to the laser axis and an annular ring of electrons residing within the pocket.

The wake at this point is in a weakly nonlinear regime

so that the toroidal pocket has not yet formed. The curvature in the wave fronts is due to a combination of nonlinear frequency shifts [32, 33] and transverse forces on the particles inside the wake. Furthermore, as seen in Fig. 3a, a group of He electrons resides near the axis just behind the first bucket. By comparing simulations with and without (not shown) N, it is clear that the formation of this line of electrons is due to the wake modification near the axis at the back of the first bucket from beam loading caused by the trapped inner-shell N electrons. The line of electrons in the second bucket modifies the transverse forces; as shown in Fig. 3b this modification results in a defocusing force region for relativistic electrons near the axis. Consequently, trapped electrons within the second bucket begin to be pushed away from the axis as they move forward into this region.

As the laser propagates further, its intensity (and ponderomotive force) increases due to photon deceleration and self-focusing. Additionally, self-trapped charge in the first bucket increases the bubble size. Therefore, by 7.5 mm (Fig. 3c) blowout and sheath splitting has begun to occur, leading to the formation of the toroidal pocket. Note that the line of He electrons in the second bucket is no longer present. Self-trapped electrons at larger radii begin to be located inside the toroidal pocket. As seen in Fig. 3d, electrons inside the pocket and on-axis are in regions of focusing (guiding) fields. Although not shown, the fields within the pocket are also accelerating the electrons and at an optimum distance electrons trapped inside the pocket form the narrowest energy ring. The field structure inside the pocket is determined by the physical structure of the sheath and streamline that form it. It results from laser and wake evolution and beam loading effects, and is essentially insensitive to the longitudinal accelerating field of the wake.

After 10 mm, the laser intensity and beam loading in the first bucket have increased. As seen in Fig. 3e, this leads to enhanced sheath splitting, while the first bucket elongates. The toroidal pocket increases in size and those electrons on-axis that run into the back of the first bucket are defocused (Fig. 3f). As a result, a clean ring of electrons is formed (as shown in Fig. 1b) that can stably propagate until it outruns the pocket. It should be noted that, although the front of the laser pulse has begun diffracting and the back is beginning to be modulated by the plasma wave at these late times (Figs. 3c and 3e), the laser is not yet pump depleted [34–36] when the ring has fully formed.

Figure 4a shows the phase space of the N K-shell electrons from the second bucket, which exhibit three characteristic features. First, close to the axis are the remaining electrons toward the back of the second bucket that have large transverse momenta and relatively lower energies. Then, at a 15 μm radius from the axis are ring electrons, which have a smaller spread of transverse momenta. The characteristic divergence angle of the ring electrons (the

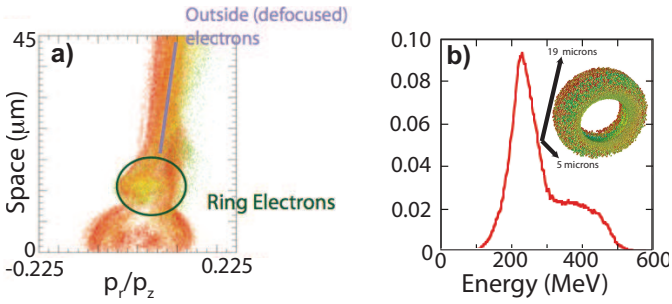

FIG. 4. After 8.8 mm of laser-propagation in the plasma, the a) phase space plot of the electrons from the second bucket and b) spectrum of the ring electrons, with an inset showing the 3-D simulation ring structure.

ratio of transverse to longitudinal momenta P_r/P_z) is $\approx$0.02 (20 mrad), which is in reasonable agreement with the experimentally-observed range of expansion angles. Finally, at large radii are the electrons that are blown out by the expanding back of the first bucket.

The longitudinal spectrum of the ring electrons is given in Fig. 4b, and their spatial structure is shown in the inset. This spectrum, which occurs after 8.8 mm of laser propagation in the simulation, demonstrates that the ring electrons are capable of attaining high energies while maintaining a finite-energy-width. Though not claiming a 1:1 correspondence between the experimental data and this simulation, the peak energy of the simulated spectrum is in excellent agreement with the experimental measurements.

Based on this physical explanation for ring formation, future work to improve the mechanism can be performed. The rings produced in both the experiment and simulations are accompanied by substantial axial electron current. To utilize these rings for applications, the ratio of the ring to axial current must be increased. One possible method is by preferentially loading charge into the second bucket (and subsequently into the ring) using a target with a density down-ramp. Another possibility is to terminate populating the first bucket by spectrally tailoring the laser pulse and allowing the bubble length to expand from the laser evolution or a density downramp. Finally, a physical stop can be placed after the plasma to block the axial current.

The process described here relies on the laser a_0 to increase sufficiently to split the electron sheath when electrons trapped in the second (or later) bucket move (dephase) into a region in which the toroidal pocket is forming. Both self- and ionization-injection can occur in the second and third buckets when these structures evolve into the blowout regime. Lasers with unmatched spot sizes but with $P/P_c \gg 1$ can evolve to matched spot sizes for which clear blowout and sheath crossing occur over a wide range of parameters. Therefore, we believe that phenomena observed in our simulation may manifest

themselves over a wide range of plasma and laser conditions. Finally, we note that it is possible to conceive of other techniques to form a ring, such as wake elongation in a density down-ramp coupled with the described laser evolution mechanism.

We thank S. H. Glenzer and J. D. Moody for useful discussions and acknowledge R. Cauble, S. Maricle, and J. Bonlie of the Callisto laser system. This work was performed under the auspices of the Department of Energy by the Lawrence Livermore National Laboratory and the University of California at Los Angeles under Contracts No. DE-AC52-07NA27344, No. DE-SC0008316, No. DE-SC0008491, and No. DE-NA0001833; NSF Grant No. ACI 1339893. This work was partially funded by the Laboratory Directed Research and Development Program under project tracking code 013-LW-076.

* electronic address: pollock6@llnl.gov

[1] G. I. Budker, Proceedings of the CERN Symposium on High Energy Accelerators (CERN, Geneva, 1956), Vol. 1, pp. 68 and 80.
[2] J.D. Lawson, Nature **218**, 430 (1968).
[3] N. Jain, T.M. Antonsen, and J.P. Palastro, ArXiv: 1410.8762v1 (2014).
[4] B. Blue et al., Phys. Rev. Lett. **90**, 214801 (2003).
[5] G. Voss and T. Weiland, "The Wake Field Acceleration Mechanism," Deutsches Electronen-Synchrotron Internal Reports, DESY M82-10 (1982) and DESY 82-079 (1982), Hamburg, Germany.
[6] G. Stancari, A. Valishev, G. Annala, G. Kuznetsov, V. Shiltsev, D.A. Still, and L.G. Vorobiev, Phys. Rev. Lett. **107**, 084802 (2011).
[7] J. Vieira and J.T. Mendonca Phys. Rev. Lett. **112**, 215001 (2014).
[8] T. Tajima and J.M. Dawson, Phys Rev. Lett. **43**, 267 (1979).
[9] C.E. Clayton et al., Phys. Rev. Lett. **105**, 105003 (2010).
[10] X. Wang et al., Nature Comm. **4**, 1988 (2013).
[11] H.T. Kim, K.H. Pae, H.J. Cha, I.J. Kim, T.J. Yu, J.H. Sung, S.K. Lee, T.M. Jeong, and J. Lee, Phys. Rev. Lett. **111**, 165002 (2013).
[12] W.P. Leemans et al., Phys. Rev. Lett. **113**, 245002 (2014).
[13] W. Lu, M. Tzoufras, C. Joshi, F.S. Tsung, W.B. Mori, J. Vieira, R.A. Fonseca, and L.O. Silva, Phys. Rev. ST Accel. Beams **10**, 061301 (2007).
[14] J.E. Ralph, K.A. Marsh, A.E. Pak, W. Lu, C.E. Clayton, F. Fang, W.B. Mori, and C. Joshi, Phys. Rev. Lett. **102**, 175003 (2009).
[15] G.-Z. Sun, E. Ott, Y.C. Lee, and P. Guzdar, Phys. Fluids **30**, 526 (1987).
[16] W. Lu, C. Huang, M. Zhou, W.B. Mori, and T. Katsouleas, Phys. Rev. Lett. **96**, 165002 (2006).
[17] A. Pak, K.A. Marsh, S.F. Martins, W. Lu, W.B. Mori, and C. Joshi, Phys. Rev. Lett. **104**, 025003 (2010).
[18] C. McGuffey et al., Phys. Rev. Lett. **104**, 025004 (2010).
[19] V. Malka et al., Science **298**, 1596 (2002).
[20] B.B. Pollock et al., Phys. Rev. Lett. **107**, 045001 (2011).
[21] I. Blumenfeld et al., Nature **445**, 741 (2007).
[22] B.B. Pollock et al., in Proc. 2009 Particle Accel Conf., (Vancouver, Canada), pp. A14: 3035-3037, IEEE, 4-8 May 2009.
[23] F. Albert et al., Phys. Rev. Lett. **111**, 235004 (2013).
[24] R. Fonseca et al., Lect. Notes Comp. Sci. **2331**, 324 (2002).
[25] C. D. Decker, and W. B. Mori, Phys. Rev. Lett. **72**, 490 (1994).
[26] M.V. Ammosov, N.B. Delone, and V.P. Krainov, Sov. Phys. JETP **64**, 1191 (1986).
[27] S.Y. Kalmykov, A. Beck, S.A. Yi, V.N. Khudik, M.C. Downer, E. Lefebvre, B.A. Shadwick, and D.P. Umstadter, Phys. Plasmas **18**, 056704 (2011).
[28] S.A. Yi, V. Khudik, S.Y. Kalmykov, and G. Shvets, Plasma Phys. Cont. Fusion **53**, 014012 (2011).
[29] M. Tzoufras, W. Lu, F. S. Tsung, C. Huang, W. B. Mori, T. Katsouleas, J. Vieira, R. A. Fonseca, and L. O. Silva, Phys. Rev. Lett. **101**, 145002 (2008).
[30] S.Y. Kalmykov et. al., New J. Phys. **14**, 033025 (2012).
[31] T. Katsouleas, Phys. Rev. A **33**, 2056 (1986).
[32] C. Joshi, W. B. Mori, T. Katsouleas, J. Dawson, J. M. Kindel, and D. W. Forslund, Nature **311**, 525 (1984).
[33] W. B. Mori, IEEE Trans. on Plasma Science, **PS − 15**, 88 (1987).
[34] B.M. Cowan et al., J. Plasma Phys. **78**, 469 (2012).
[35] E.N. Nerush and I.Y. Kostyukov, Phys. Rev. Lett. **103**, 035001 (2009).
[36] A.F. Lifschitz and V. Malka, New J. Phys. **14**, 053045 (2012).